

Multichannel Regularized Iterative Restoration of Motion Compensated Image Sequences

Mun Gi Choi*, Nikolas P. Galatsanos*, and Aggelos K. Katsaggelos**

*Department of Electrical and Computer Engineering
Illinois Institute of Technology, Chicago, IL 60616
Tel. (312)567-5259, e-mail : npg@ece.iit.edu

**Department of Electrical Engineering and Computer Science
Northwestern University, Evanston, IL 60208

Multichannel Regu. Iter. Restor. of Motion Compen. Imag. Seq.

Nikolas P. Galatsanos

Department of Electrical and Computer Engineering
Illinois Institute of Technology, Chicago, IL 60616
Tel. (312)567-5259, e-mail : npg@ikaria.iit.edu

Abstract

Restoration of image sequences is an important problem that can be encountered in many image processing applications, such as, visual communications, robot guidance and target tracking. The independent restoration of each frame in an image sequence is a suboptimal approach because the between-frame correlations are not explicitly taken into consideration. In this paper we address this problem by proposing a multichannel restoration approach. The multiple time-frames (channels) of the image sequence are restored simultaneously by using a multichannel regularized least-squares formulation of the problem. The regularization operator captures both within and between-frame (channel) properties of the image sequence with the explicit use of the displacement vector field. We propose a number of different approaches to obtain the multichannel regularization operator, as well as, an algorithm to iteratively compute the restored images. We present experiments that demonstrate the value of the proposed multichannel approach.

- N : Capital Italic
- M : Capital Italic
- g_i : Italic
- H_i : Capital Italic
- f_i : Italic
- n_i : Italic
- \mathbf{g} : Bold
- \mathbf{f} : Bold
- \mathbf{n} : Bold
- \mathbf{H} : Bold Capital
- \mathbf{J} : Bold Capital
- \mathbf{Q} : Bold Capital
- $\hat{\mathbf{f}}$: Bold
- λ_i : Greek Lowercase
- Σ : Greek Uppercase
- $\mathbf{\Lambda}$: Bold Greek Uppercase
- \mathbf{I} : Bold Capital
- \mathbf{Q}_{3-DWL} : Bold Capital
- Q_{ij} : Capital Italic
- q_{ij} : Italic
- $f^l(i, j)$: Italic

- $x_{i,j}$: Italic
- (i, j) : Italic
- l : Italic
- $m_{(l,l)}^{(i,j)}$: Italic
- $n_{(l,l)}^{(i,j)}$: Italic
- **Q3-DMCL** : Bold Capital
- k : Italic
- **y** : Bold
- **z** : Bold
- $y^l(i, j)$: Italic
- **A** : Bold Capital
- **$\hat{\mathbf{f}}_k$** : Bold
- α : Greek Lowercase
- μ_{max} : Greek Lowercase
- X_k : Capital Italic
- **B** : Bold Capital
- μ'_k : Greek Lowercase
- σ^2 : Greek Lowercase
- $h(i, j)$: Italic
- $f_j^{(i)}$: Italic

1 Introduction

Degradation of image sequences can occur during the recording, sensing, transmission and storage stages. Since the degraded sequence has lost information, a restoration process that will recover some of the lost information can be very useful in many applications where such sequences are used. Visual communications is probably the most prominent application that could benefit directly from advances in image sequence restoration. However, many other applications where image sequences are used can also benefit from the restoration results described in this work, as for example, remote sensing, robot guidance and search/detection of targets.

Image sequences are signals with very strong temporal correlation. This temporal correlation is an important defining feature of such signals, and has been used for their compact representation. Indeed for image sequence compression there is a wide consensus among researchers that the between-frame correlation, which is captured by the displacement-vector-field (DVF), is an indispensable feature [15] and [14]. Image restoration is an ill-posed problem; regularization has to be used to ameliorate the effects of the noise and the ill-posed nature of the blurring operator [19], [9] and [8]. Regularization refers to a class of methods according to which the image is recovered using both the observed data and *prior known properties* of the original image. Since image sequences exhibit strong temporal correlation, it is clear that this information must be used in the regularization process of a restoration algorithm if optimal results are desired.

We define as *multichannel images* the multiple image planes (channels) obtained by an imaging system that measures the same scene using multiple sensors. By definition multichannel images exhibit strong between-channel correlations. Therefore, processing them as one entity is very important because both the *within* and *between*-channel correlations are used. In the rest of this paper we shall refer to this type of processing as *multichannel*.

Based on the previous definition, it is clear that image sequences are multichannel signals. In this case the channels are the different time-frames of the sequence. Other examples of multichannel images are multispectral/color images. In this case the channels are the different spectral components red (R), green (G) and blue (B) of the color image. The literature of multichannel restoration for multispectral/color images is quite mature. This problem was first proposed in [10] where the separability of the spatial and spectral correlations was used in order to derive multichannel linear minimum mean square error (LMMSE) filters. In [5], [6] and [7] this separability assumption was relaxed and stochastic multichannel restoration filters were

proposed. In [7] and [21] regularization was used to obtain deterministic multichannel constrained least squares (CLS) filters that avoid some of the difficulties of the stochastic filters in [5] and [6]. Recently, constrained minimum mean square error (CMMSE) filters were also proposed in [20] for this problem. The CMMSE formulation combines a stochastic LMMSE criterion with a deterministic CLS error criterion.

Both color/multispectral and image sequences fall under the broad definition of multichannel signals. However, for color/multispectral images the channels are registered, thus, the between-channel correlation can be captured by a space-invariant regularization operator [5], [6], [7] and [21]. In contrast, image sequences are not registered, furthermore, their between-channel correlation (DVF) is space-variant. Therefore, their between-channel correlation cannot be captured by a space-invariant regularization operator. If space-variant regularization is used the restoration filter cannot be implemented in the discrete frequency domain using the algorithms in [5], [6], [17] and [13]. In addition, since the DVF is not known a priori, the exact form of the regularization operator is not known.

A first attempt to restore image sequences as multichannel signals can be found in [17]. For this purpose multichannel LMMSE filters were proposed that assumed *uniform motion* over the entire image. This assumption bypassed the main difficulty of this problem and the proposed multichannel filters were computed in closed form using the algorithms in [5], [7], [17] and [13]. However, this assumption is extremely limiting since image sequences with uniform motion are encountered in few specialized applications. The multichannel approach was also used in [1] for filtering motion compensated image sequences corrupted by Poisson noise. In [1] no blurring was assumed and a stochastic solution approach was used.

In this paper we propose a family of least-squares multichannel restoration filters that use a space-variant regularization operator to capture the between-channel correlations of image sequences. This, gives us the capability to enforce smoothness *both* spatially and the temporal direction and thus take full advantage of the available data. Although this seems to be a very natural idea in the context of this problem, to the best of our knowledge, this is the first time that it has been implemented. We provide numerical experiments that show beyond any doubt that this idea works very well.

Since the DVF is unknown, an estimate is used to define the regularization operator. Such estimates are initially obtained either from the noisy-blurred images directly, or from the restored image sequences without motion compensation. These estimates can be further refined by

repeated steps of DVF estimation and multichannel restoration. As already mentioned above, since a space-variant regularization operator is used, the algorithms proposed in [7], [17] and [13] can not be used to compute the restored images in closed form. Thus, in this paper an iterative algorithm is used for the implementation of the proposed multichannel restoration filters.

The rest of this paper is organized as follows. In section 2 we introduce notation and review the theory of regularized least-squares restoration of multichannel images with registered channels. This approach is extended in section 3 to image sequences. Image sequences are multichannel images with non-registered channels. In section 3 we introduce a new multichannel regularization operator that captures both the within-channel (spatial) and the between-channel (temporal) properties of image sequences. In section 4 we propose an iterative algorithm for the computation of the regularized least-squares solution and convergence issues of this algorithm are discussed. In section 5 we present experimental results. Finally, in section 6 we present our conclusions from this work.

2 Regularized Least Squares Multichannel Restoration

In this paper we assume a discrete linear imaging model with N channels. Such a model is described by

$$g_i = H_i f_i + n_i, \text{ for } i = 1, 2, \dots, N, \quad (1)$$

where g_i , f_i and n_i represent the lexicographically ordered i -th observed image, original image and additive random noise, respectively, each a $M^2 \times 1$ vector, and H_i denotes the linear spatially invariant or spatially varying degradation operator. By stacking the $M^2 \times 1$ vectors g_i , f_i and n_i we obtain

$$\mathbf{g} = \begin{bmatrix} g_1 \\ g_2 \\ \vdots \\ g_N \end{bmatrix}, \quad \mathbf{f} = \begin{bmatrix} f_1 \\ f_2 \\ \vdots \\ f_N \end{bmatrix}, \quad \mathbf{n} = \begin{bmatrix} n_1 \\ n_2 \\ \vdots \\ n_N \end{bmatrix}. \quad (2)$$

Thus Eq. (1) can be rewritten as

$$\mathbf{g} = \mathbf{H}\mathbf{f} + \mathbf{n}, \quad (3)$$

where

$$\mathbf{H} = \text{diag}\{H_1, H_2, \dots, H_N\} \quad (4)$$

is the $NM^2 \times NM^2$ multichannel degradation matrix and \mathbf{g} , \mathbf{f} and \mathbf{n} denote the lexicographically ordered multichannel vectors of size $NM^2 \times 1$.

Using the constrained least squares regularization approach an estimate $\hat{\mathbf{f}}$ is obtained by minimizing

$$\mathbf{J}(\mathbf{f}) = \sum_{i=1}^N \frac{1}{\lambda_i} \|\overline{H}_i \mathbf{f} - g_i\|^2 + \|\mathbf{Q}\mathbf{f}\|^2, \quad (5)$$

where $\overline{H}_i = [0, \dots, 0, H_i, 0, \dots, 0]$ and λ_i represent the regularization parameter corresponding to the i -th channel [7]. The multichannel estimate $\hat{\mathbf{f}}$ is given in closed form by

$$\hat{\mathbf{f}} = (\mathbf{H}^t \mathbf{H} + \Lambda \mathbf{Q}^t \mathbf{Q})^{-1} \mathbf{H}^t \mathbf{g}, \quad (6)$$

with the matrix Λ defined as

$$\Lambda = \begin{bmatrix} \lambda_1 [\mathbf{I}] & 0 & 0 & \cdots & 0 \\ 0 & \lambda_2 [\mathbf{I}] & 0 & \cdots & \vdots \\ 0 & 0 & \ddots & 0 & \vdots \\ \vdots & \vdots & 0 & \ddots & 0 \\ 0 & \cdots & \cdots & 0 & \lambda_N [\mathbf{I}] \end{bmatrix}, \quad (7)$$

where $[\mathbf{I}]$ are $M^2 \times M^2$ identity matrices and \mathbf{Q} is the multichannel regularization operator [7]. The role of \mathbf{Q} is to enforce both within and between-channel smoothness in the restored image. The values of the regularization parameters define the degree to which smoothness is enforced [7].

For the multichannel restoration of R, G and B color images the 3-D weighted Laplacian was used as the regularization operator in [7] and [21]. This operator assumes both spatial and spectral smoothness of the original image and can be represented by the following block matrix

$$\mathbf{Q}_{3\text{-DWL}} = \begin{bmatrix} Q_{11} & Q_{12} & Q_{13} \\ Q_{21} & Q_{22} & Q_{23} \\ Q_{31} & Q_{32} & Q_{33} \end{bmatrix}. \quad (8)$$

Since both spatial and spectral relations within channels are assumed to be space-invariant, the submatrices Q_{ii} and Q_{ij} ($i \neq j$) represent 2-D convolution with 3×3 masks q_{ii} and q_{ij} centered at (0,0) and given respectively by

$$q_{ii} = \begin{bmatrix} 0 & 1 & 0 \\ 1 & -6 & 1 \\ 0 & 1 & 0 \end{bmatrix}, \quad q_{ij} = \begin{bmatrix} 0 & 0 & 0 \\ 0 & x_{i,j} & 0 \\ 0 & 0 & 0 \end{bmatrix}, \quad (9)$$

$i, j = 1, 2, 3$. The scalar $x_{i,j}$ captures the between color channel intensity relation which is assumed space-invariant [7] and [21]. Thus, when $\mathbf{Q}_{3\text{-DWL}}$ is applied to a multichannel image \mathbf{f}

the result at the (i, j) spatial location in the l -th channel is equal to

$$[\mathbf{Q}_{\mathbf{3-DWL}} \mathbf{f}]_{(i,j)}^l = -6f^l(i, j) + f^l(i-1, j) + f^l(i+1, j) + f^l(i, j-1) + f^l(i, j+1) \\ + x_{l,l-1}f^{l-1}(i, j) + x_{l,l+1}f^{l+1}(i, j), \quad \text{for } i, j = 1, 2, \dots, M. \quad (10)$$

The choice of the 3-D weighted Laplacian as a regularization operator for the color image restoration problem is justified by the fact that the R, G, and B channels are completely registered. In other words, the (i, j) pixel in one channel corresponds to the (i, j) pixel in all other channels. Therefore, a 3-D space-invariant operator like the 3-D weighted Laplacian captures effectively both the within and between-channel relations of color images [7] and [21].

For N channels each of size $M \times M$, when circulant convolution is assumed, $\mathbf{Q}_{\mathbf{N-DWL}}$ is a $NM^2 \times M^2N$ matrix. This matrix contains circulant submatrices Q_{ij} each of size $M^2 \times M^2$, but it is not circulant since $Q_{ij} \neq Q_{i+k, j+k}$. For a realistic imaging problem, i.e. $M=256$ and $N=3$, the size of the matrix that has to be inverted in Eq. (6) is $196,608 \times 196,608$. Matrices of this size are too large to be handled even with present computer technology. Therefore, the special structure of these matrices must be exploited in order to compute $\hat{\mathbf{f}}$ from Eq. (6). In [7], [17] and [13] a family of algorithms was proposed that allows the efficient closed form computation of $\hat{\mathbf{f}}$ from Eq. (6) in the discrete frequency domain.

3 Multichannel Regularization of Image Sequences

In image sequences, pixel (i, j) in one frame does not necessarily correspond to pixel (i, j) in the neighborhood frames. Assuming integer motion, pixel (i, j) in frame (l) will correspond to pixel $(i + m_{(l-1,l)}^{(i,j)}, j + n_{(l-1,l)}^{(i,j)})$ in frame $(l-1)$, where the integer $(m_{(l-1,l)}^{(i,j)}, n_{(l-1,l)}^{(i,j)})$ express the horizontal and vertical motion between the $(l-1)$ and (l) -th frames, respectively, at the (i, j) spatial location. Using a similar notation the correspondence of pixel (i, j) in frame (l) and $(l+1)$ can be expressed. In *Figure 1* this between-frame correspondence is shown pictorially.

Furthermore, in real image sequences the motion is not space-invariant. In other words, the vector $(m_{(l-1,l)}^{(i,j)}, n_{(l-1,l)}^{(i,j)})$ changes from pixel-to-pixel. Thus, the between-channel smoothing operators Q_{ij} for $i \neq j$ used for R, G, B color images and described by Eq. (10) are not appropriate for the image sequence restoration problem because they fail to capture the space-variant nature of the motion.

For this purpose we propose a new regularization operator called the N-D motion compensated Laplacian (MCL). For $N = 3$ this operator, as the previously defined $\mathbf{Q}_3\text{-DWL}$ is a $3M^2 \times 3M^2$ block-matrix and is denoted by $\mathbf{Q}_3\text{-DMCL}$. The application of this operator to a multichannel image \mathbf{f} is described by

$$[\mathbf{Q}_3\text{-DMCL } \mathbf{f}]_{(i,j)}^l = -6f^l(i,j) + f^l(i-1,j) + f^l(i+1,j) + f^l(i,j-1) + f^l(i,j+1) + f^{l-1}\left(i + m_{(l-1,l)}^{(i,j)}, j + n_{(l-1,l)}^{(i,j)}\right) + f^{l+1}\left(i + m_{(l+1,l)}^{(i,j)}, j + n_{(l+1,l)}^{(i,j)}\right), \quad (11)$$

where l is again the channel index, (i,j) denotes the spatial location and $(m_{(l+k,l)}^{(i,j)}, n_{(l+k,l)}^{(i,j)})$ for $k = -1, 1$ represent the DVF between l and $(l+k)$ -th frames at the spatial location (i,j) . From the definition of $\mathbf{Q}_3\text{-DMCL}$ in Eq. (11) it is clear that this operator first compensates for the motion between-frames and then enforces both within and between-channel smoothness.

The operator $\mathbf{Q}_3\text{-DMCL}$ is a block matrix that can also be described by Eq. (8). However, in the case of $\mathbf{Q}_3\text{-DMCL}$ submatrices Q_{ij} for $i \neq j$ are *not circulant*. Thus, direct computation of $\hat{\mathbf{f}}$ from Eq. (6) is impossible since the frequency domain techniques described in [7] and [13] are not applicable and direct inversion of the matrix $(\mathbf{H}^t\mathbf{H} + \Lambda\mathbf{Q}^t\mathbf{Q})$ is required. In what follows an iterative method is proposed for the computation of $\hat{\mathbf{f}}$.

4 An Iterative Algorithm to Compute $\hat{\mathbf{f}}$

The restored image $\hat{\mathbf{f}}$ is the solution of the linear system of equations

$$(\mathbf{H}^t\mathbf{H} + \Lambda\mathbf{Q}^t\mathbf{Q})\hat{\mathbf{f}} = \mathbf{H}^t\mathbf{g}. \quad (12)$$

The direct computation of $\hat{\mathbf{f}}$ from Eq. (12) is not possible since for $\mathbf{Q} = \mathbf{Q}_3\text{-DMCL}$ the matrix $\mathbf{A} = \mathbf{H}^t\mathbf{H} + \Lambda\mathbf{Q}^t\mathbf{Q}$ does not have a special structure that will allow for its inversion, as in the multichannel color image case. However, since it is possible to compute the product $(\mathbf{H}^t\mathbf{H} + \Lambda\mathbf{Q}^t\mathbf{Q})\mathbf{y}$ where \mathbf{y} is a known vector *iterative methods* can be used to solve Eq. (12).

The product $(\mathbf{H}^t\mathbf{H} + \Lambda\mathbf{Q}^t\mathbf{Q})\mathbf{y}$ can be broken into $\mathbf{H}^t\mathbf{H}\mathbf{y} + \Lambda\mathbf{Q}^t\mathbf{Q}\mathbf{y}$. The first term is straightforward to compute. For the second term we need to compute both $\mathbf{Q}\mathbf{y}$ and $\mathbf{Q}^t\mathbf{z}$ where $\mathbf{z} = \mathbf{Q}\mathbf{y}$. For $\mathbf{Q} = \mathbf{Q}_3\text{-DMCL}$ from Eq. (11) we can write

$$[\mathbf{Q}_3\text{-DMCL } \mathbf{y}]_{(i,j)}^l = \left[-4y^l(i,j) + y^l(i-1,j) + y^l(i+1,j) + y^l(i,j-1) + y^l(i,j+1)\right] + \left[y^{l-1}\left(i + m_{(l-1,l)}^{(i,j)}, j + n_{(l-1,l)}^{(i,j)}\right) - y^l(i,j)\right] + \left[y^{l+1}\left(i + m_{(l+1,l)}^{(i,j)}, j + n_{(l+1,l)}^{(i,j)}\right) - y^l(i,j)\right]. \quad (13)$$

The terms inside the first bracket of the right hand side of Eq. (13) is the convolution of each channel of y^l with the 2-D Laplacian operator. The terms inside the second and third brackets represent the motion compensated prediction errors between the pair of frames $(l-1, l)$ and $(l+1, l)$, respectively. The multichannel regularization matrix used in this paper is symmetric, i.e. $\mathbf{Q}_{3\text{-DMCL}} = \mathbf{Q}_{3\text{-DMCL}}^T$. Thus, $\mathbf{Q}^t \mathbf{z}$ can be computed similarly as $\mathbf{Q} \mathbf{y}$. In Appendix A we elaborate in detail on the assumptions that yield this symmetry.

The successive approximations based iteration [18] for solving Eq. (12) is given by

$$\hat{\mathbf{f}}_0 = \mathbf{0} \quad (14)$$

$$\hat{\mathbf{f}}_{k+1} = \hat{\mathbf{f}}_k + \alpha (\mathbf{H}^t \mathbf{g} - (\mathbf{H}^t \mathbf{H} + \Lambda \mathbf{Q}^t \mathbf{Q}) \hat{\mathbf{f}}_k), \quad (15)$$

where α , the *relaxation parameter*, is a scalar that controls the convergence properties of this iteration. It is easy to check that a stationary point of this iteration satisfies Eq. (12). However, in order for an iteration to have a unique *stationary point* the mapping defined by this iteration must be a contraction mapping [16].

With $\mathbf{A} = \mathbf{H}^t \mathbf{H} + \Lambda \mathbf{Q}^t \mathbf{Q}$ and $\|\cdot\|$ the l_2 norm one can show, see for example [18] and [12], that Eq. (15) is a contraction mapping when

$$\|\mathbf{I} - \alpha \mathbf{A}\| < \mathbf{1}. \quad (16)$$

Since \mathbf{A} is a symmetric and positive definite matrix, the inequality in Eq. (16) is satisfied if

$$\alpha \mu_{max} < 2, \quad (17)$$

where μ_{max} is the largest eigenvalue of \mathbf{A} . Therefore, the bounds for α in order to ensure the convergence of the iteration in Eq. (15) are given by

$$0 < \alpha < \frac{2}{\mu_{max}}. \quad (18)$$

Because of the size and structure of \mathbf{A} in our application, the analytic computation of μ_{max} is not feasible. Therefore, we use a method based on the Rayleigh quotient iteration to compute μ_{max} numerically [3].

Consider the iteration

$$X_{k+1} = \mathbf{B} X_k, \text{ for } k = 0, 1, 2 \dots \quad (19)$$

where \mathbf{B} is a symmetric $K \times K$ matrix, and the ratio

$$\mu'_k = \frac{(X_{k+1})^t X_k}{(X_k)^t X_k}, \quad (20)$$

where t denotes the transpose of a vector and X_0 any vector $\in R^k$ which is not an eigenvector of \mathbf{B} or the zero-vector. Then, it can be shown that for $k \rightarrow \infty$, $\mu'_k \rightarrow \mu_{max}$, where μ_{max} is the largest in magnitude eigenvalue of \mathbf{B} [3]. Furthermore, it can be shown that $\mu'_k > \mu_{max}$, $\forall k$ [3]. If the value of the relaxation parameter used in Eq. (15), is chosen as

$$\alpha = \frac{2}{\mu'_k}, \quad (21)$$

for some large k , then this value always satisfies the bounds of Eq. (18).

5 Experiments

Experiments were performed to test the proposed iterative multichannel restoration algorithm. Ten frames (each of size 256×256) from the "Trevor White" sequence were used as test images. The results obtained with the proposed algorithm are compared with the results obtained by restoring each frame separately (henceforth referred to Model 0). The single channel version of Eq. (6) was used with \mathbf{Q} , the 2-D Laplacian. In order to apply iteration in Eq. (15) the DVF needs to be estimated first. Four different approaches were used for this task. Each of these approaches, along with iteration in Eq. (15), is henceforth referred to as Model 1 - Model 4. More specifically :

(1) Model 1 : The DVF was estimated directly from the degraded images.

(2) Model 2 : The DVF was estimated from the images restored by Model 0.

(3) Model 3 : The DVF was estimated from the images restored by Model 2.

(4) Model 4 : The original image sequence is used to obtain the DVFs. This model is used to test the upper bound of performance of the proposed multichannel restoration algorithm.

For Models 1, 2 and 3 the DVF is computed from either the degraded or the restored images. Since pel-recursive algorithms are more sensitive to artifacts in the degraded or the restored images, a block search algorithm (BSA) was used to estimate the between-channel DVFs. The

motion vector at pixel (i, j) between frames, l and k , was found by matching a 5×5 window centered at pixel (i, j) of frame l to a 5×5 window in frame k . An exhaustive search over 31×31 area centered at pixel (i, j) of frame k was used and the matching metric was the sum of the squared errors.

It is clear that the more strongly-correlated channels are available the better the restoration results, if a multichannel approach is used. However, as a general rule, as the time separation between frames in an image sequence increases, the correlation between-frames decreases. Thus, it is expected that after a certain number of frames the improvements due to the inclusion of additional frames diminish. In addition to this, the computational cost of the proposed algorithm for N channels is proportional to N^3 . Taking all the above considerations into account $N = 5$ was chosen for our experiments.

Two experiments are presented in this paper (more experiments can be found in [2] and [4]). In the experiments presented in this paper all five models were tested and compared. The variance of the noise added to the blurred data is defined using the blurred signal-to-noise ratio ($BSNR$) metric which is given by

$$BSNR = 10 \log_{10} \frac{\|\overline{Hf} - Hf\|^2}{M^2 \sigma^2} dB, \quad (22)$$

where σ^2 is the variance of the additive noise, M^2 is the total numbers of pixel in the image, and \overline{Hf} is the spatial mean of the blurred image Hf . As an objective measure of performance of the restoration algorithms the improvement signal-to-noise ratio ($ISNR$) metric was used. This metric is defined by

$$ISNR = 10 \log_{10} \frac{\|f - g\|^2}{\|f - \hat{f}\|^2} dB, \quad (23)$$

where f , g and \hat{f} are the original image, the degraded image and the restored image, respectively. In all experiments the relaxation parameter α was obtained numerically using the Rayleigh quotient based method described in section 4. The value of each of the regularization parameters λ_i was chosen to be equal to $\left(10^{\frac{BSNR}{10}}\right)^{-1}$ [7], [21]. To restore all ten frames of the image sequence six five-channel multichannel filters were used. Except for the first and last two frames of the sequence a five-channel non-causal filter was used to restore each frame. This filter used both the two previous and the two following frames of the frame under restoration.

Experiment I

In this experiment ten frames (frames 41-50) of the Trevor White sequence were blurred by

an 11×11 uniform blur. The point spread function of this blur is given by

$$h(i, j) = \begin{cases} \frac{1}{121} & \text{if } -5 \leq i, j \leq 5 \\ 0 & \text{otherwise.} \end{cases} \quad (24)$$

Cases (i), and (ii) corresponding to 10 and 30 dB *BSNR* respectively of additive white Gaussian noise were examined. In *Figures 2, 5* and *11* *ISNR* plots are shown, while in *Figures 3, 6* and *12* the displaced-frame difference (*DFD*) is shown for both cases. The *DFD* is defined as

$$DFD = 10 \log_{10} \frac{\|f_k - f_k'\|^2}{M^2} dB, \quad (25)$$

where M^2 is the total numbers of pixel in the image, and f_k' is the motion compensated estimate of frame f_k using all the DVFs used for the restoration of the frame f_k . For example, for $N = 5$,

$$f_j' = \frac{1}{4}[f_j^{(j-2)} + f_j^{(j-1)} + f_j^{(j+1)} + f_j^{(j+2)}], \quad (26)$$

where $f_j^{(i)}$ is the motion compensated estimates of f_j using frame i and the DVF between frames i and j .

In *Figures 8, 9* and *10* the 8th frame of this experiment is shown for cases (i) and (ii). The original and the degraded images are shown in *Figure 8*. In *Figures 9* and *10* the restored images from this experiment are shown.

The *DFD* plots for this experiment when compared with the *ISNR* plots clearly point out that the more accurate the motion estimation the better the restoration. From the *ISNR* and the *DFD* plots it is also clear that for both cases *BSNR* (10, 30 dB) estimating the motion from the restored images (Models 2 and 3) is clearly superior to using the degraded images directly (Model 1). This can also be verified by visually inspecting the restored images in *Figures 9(b)* and *9(c)*.

Needle plots for DVF are shown to visualize the actual motion estimates for the 10 dB and 30 dB noise cases in *Figure 4* and *7*, respectively. At this point we have to make an important observation that was brought up during the review process. Finding the motion of a scene is a very ill-posed problem. Therefore, from the degraded or the restored frames available, we have no hope in estimating accurately the motion in this scene, see for example the needle plots in *Figure 4(a)* and *7(a)*. Even with the original image, the block matching algorithm that we use does not provide a good estimate of the motion field of this scene, see *Figure 4(d)*. However, for our application we do not need a good motion field estimate what we need is an *approximate*

direction of temporal correlation. This, we can get from the degraded or restored images available using a full search block matching algorithm for each pixel. The *DFD* results shown in *Figure 3* and *6*. confirm this observation.

Experiment II

In this experiment the same ten frames as in Experiment I were used. However, this time each frame was blurred by a different size blur simulating the blur that would occur by the accelerating-decelerating motion of a recording camera. Uniform horizontal motion blurs of size 3×1 , 5×1 , 7×1 , 9×1 , 11×1 , 11×1 , 9×1 , 7×1 , 5×1 and 3×1 were used to blur frames 1, 2, 3, 4, 5, 6, 7, 8, 9, and 10 respectively. 30 dB *BSNR* of additive white Gaussian noise was examined. In *Figure 11* the *ISNR* results from this experiment are plotted. In *Figure 12* the *DFD* plots are given. Original and degraded images are shown in *Figure 13*, while restored images from this experiment are shown in *Figure 14*.

In both of our experiments we observed that the value of the relaxation parameter decreased as the *BSNR* increases (see for example the α values in *Figures 2* and *5*). This is explained by the fact that since $\mathbf{Q}^t\mathbf{Q}$ is a positive definite matrix the value of the largest eigenvalue μ_{max} of the matrix $\mathbf{A} = \mathbf{H}^t\mathbf{H} + \lambda\mathbf{Q}^t\mathbf{Q}$ increases with λ . Furthermore, α is inversely proportional to μ_{max} . We also observed that the number of iterations required to find the stationary point of Eq. (15) increases as the *BSNR* increases. For example, in experiment I in the case of *BSNR* = 10 dB, 40 iterations were required whereas in case of *BSNR* = 30 dB, 110 iterations were required. This can be explained by the fact that the *condition number* of the matrix \mathbf{A} given by the ratio $\frac{\mu_{max}}{\mu_{min}}$ where μ_{min} and μ_{max} are the smallest and largest eigenvalues of \mathbf{A} , respectively, decreases as λ increases. Larger values of λ corresponds to more regularization, in other words, a better conditioned matrix \mathbf{A} . However, it is well known that the smaller the condition number of a matrix the faster the successive approximation iterations given by Eq. (15) converge [3].

6 Conclusions

In this paper multichannel least squares filters were used for the regularized restoration of image sequences. It was found that the multichannel filters which enforce both spatial and temporal smoothness along the direction of the motion give by far superior results both visually and using a mean square error metric, over the single-channel restoration filters that only enforce spatial

smoothness. Our experiments also demonstrated that the accuracy with which the direction of the temporal correlation can be found is crucial to the quality of the multichannel restored images. We also found that if the direction of the temporal correlation is found from the original sequence (even with the integer motion assumption) the multichannel restored image (Model 4) for *BSNRs* ranging from [10 and 30] *dB* is almost identical to the original image.

7 Acknowledgements

The authors, especially the first one, are grateful to Dr. Yongyi Yang, at the ECE Dept. of the Illinois Institute of Technology for suggesting the power method to estimate the relaxation parameter α .

8 Appendix A

In this appendix the assumptions that result in a symmetric multichannel regularization operator $\mathbf{Q}_{3\text{-DMCL}}$ as discussed. To simplify notation and without loss of generality $N = 3$ is used. Then, this operator $\mathbf{Q}_{3\text{-DMCL}}$ is given by

$$\mathbf{Q}_{3\text{-DMCL}} = \begin{bmatrix} \mathbf{Q} & \mathbf{M}_l^{l+1} & \mathbf{M}_{l-1}^{l+1} \\ \mathbf{M}_{l+1}^l & \mathbf{Q} & \mathbf{M}_{l-1}^l \\ \mathbf{M}_{l+1}^{l-1} & \mathbf{M}_l^{l-1} & \mathbf{Q} \end{bmatrix}, \quad (27)$$

where all the entries of the right-hand-side for $M \times M$ images are $M^2 \times M^2$ matrices. \mathbf{Q} is the matrix that represents the convolution of a $M \times M$ image with the kernel

$$\mathbf{q} = \begin{bmatrix} 0 & 1 & 0 \\ 1 & -6 & 1 \\ 0 & 1 & 0 \end{bmatrix}, \quad (28)$$

and \mathbf{M}_j^i for $m = l - 1, l, l + 1$ are the motion compensation matrices. In other words,

$$\hat{\mathbf{X}}_i = \mathbf{M}_j^i \mathbf{X}_j \quad (29)$$

where $\hat{\mathbf{X}}_i$ is the motion compensated estimate of frame i when frame j is used. \mathbf{Q} is symmetric since it represents a convolution with a symmetric kernel. Furthermore, we will demonstrate using an example that

$$\mathbf{M}_j^i{}^T = \mathbf{M}_i^j \quad (30)$$

Assuming perfect motion compensation the two frames i and j are related via the following matrix-vector equation.

$$\mathbf{X}_i = \mathbf{M}_j^i \mathbf{X}_j. \quad (31)$$

To better illustrate the properties of matrix \mathbf{M}_j^i , without loss of generality we show a simple 2×2 image.

The assumption that is made in this paper is that the same pixel from frame j cannot be used to compensate more than one pixel of frame i . Using the lexicographic ordering the following equation is an example of what this assumption would imply for matrix \mathbf{M}_j^i . For this example Eq. (31) in detail gives

$$\begin{bmatrix} X_i(1,1) \\ X_i(2,1) \\ X_i(1,2) \\ X_i(2,2) \end{bmatrix} = \begin{bmatrix} 0 & 1 & 0 & 0 \\ 0 & 0 & 1 & 0 \\ 1 & 0 & 0 & 0 \\ 0 & 0 & 0 & 1 \end{bmatrix} \begin{bmatrix} X_j(1,1) \\ X_j(2,1) \\ X_j(1,2) \\ X_j(2,2) \end{bmatrix}. \quad (32)$$

This assumption yields an \mathbf{M}_j^i which is an *indicator matrix* of full rank. Thus, the following equation holds

$$\left(\mathbf{M}_j^i\right)^T \mathbf{M}_j^i = \mathbf{I}. \quad (33)$$

Then, from Eq. (31) and (33) we get

$$\mathbf{X}_j = \left(\mathbf{M}_j^i\right)^T \mathbf{X}_i. \quad (34)$$

in other words, $\left(\mathbf{M}_j^i\right)^T = \mathbf{M}_i^j$. Therefore, $\mathbf{Q}_{3-DMCL} = \mathbf{Q}_{3-DMCL}^T$. This assumption is without doubt limiting, however, it greatly simplifies the calculation of the filter.

References

- [1] C. L. Chan, A. K. Katsaggelos and A. V. Sahakian, Image Sequence Filtering in Quantum-Limited Noise with Applications to Low-Dose Fluoroscopy, *IEEE Trans. on Medical Imaging*, Vol. 12, No. 3, Sept. 1993, pp. 610-621.
- [2] Mun Gi Choi, Multichannel Regularized Iterative Restoration of Image Sequences, M.S. Thesis, Illinois Institute of Technology, Chicago, IL, August 1993.
- [3] S. D. Conte and C. de Boor, Elementary Numerical Analysis, *McGraw-Hill Book Company* 1980.
- [4] Ozan E. Erdogan, A Multichannel Regularized Iterative Algorithm for the Restoration of Noisy and Blurred Image Sequences, M.S. Thesis, Northwestern University, Evanston, IL, June 1993.
- [5] N. P. Galatsanos and R. T. Chin, Digital Restoration of Multichannel Images, *IEEE Trans. Acoustics, Speech and Signal Processing*, Vol. 37, No. 3, March 1989.
- [6] N. P. Galatsanos and R. T. Chin, Restoration of Color Images by Multichannel Kalman Filtering, *IEEE Trans. Signal Processing*, vol. ASSP-39, no. 10, Oct. 1991, pp. 2237-2252.
- [7] N. P. Galatsanos, A. K. Katsaggelos, R. T. Chin and A. D. Hillery, Least Squares Restoration of Multichannel Images, *IEEE Trans. Signal Processing*, Vol. 39, No. 10, Oct. 1991, pp. 2222-2236.

- [8] N. P. Galatsanos, and A. K. Katsaggelos, Methods for Choosing the Regularization Parameter and Estimating the Noise variance in Image Restoration and their Relation, *IEEE Trans. on Image Processing*, Vol. 1, No. 3, July 1992, pp. 322-336.
- [9] B. R. Hunt, The Application of Constrained Least Squares Estimation to Image Restoration by Digital Computer, *IEEE Trans. Computers*, Vol. 22, No. 9, Sept. 1973, pp. 805-812.
- [10] B. R. Hunt and O. Kubler, Karhunen-Loeve Multispectral Image Restoration, Part I: Theory, *IEEE Trans. Acoustics, Speech and Signal Processing*, Vol. ASSP-32, No. 3, June 1984, pp. 592-600.
- [11] A. K. Katsaggelos, Iterative Image Restoration Algorithms, *Opt. Eng.*, vol. 28, no. 7, July 1989, pp. 735-748.
- [12] A. K. Katsaggelos, J. Biemond, R. W. Schafer and R. M. Mersereau, A Regularized Iterative Image Restoration Algorithm, *IEEE Trans. Signal Processing*, Vol. 39, No. 4, April 1991, pp. 914-929.
- [13] A. K. Katsaggelos, K. T. Lay, and N. P. Galatsanos, A General Framework for Frequency Domain Multichannel Signal Processing, *IEEE Trans. Image Proc.*, vol. 2, no. 3, July 1993, pp. 417-420.
- [14] D. LeGall, MPEG-A Video Compression Standard for Multimedia Applications, *Communications of the ACM*, Vol. 34, No. 4, April 1991, pp. 46-58.
- [15] H. Musmann, P. Pirsch, H. Grallert, Advances in Picture Coding, *Proc. IEEE*, April 1985, pp. 523-542.
- [16] J. M. Ortega and W.C. Rheindoldt, Iterative Solution of Nonlinear Equations in Several Variables, *Academic Press*, 1970.
- [17] M. K. Ozkan, A.T. Erdem, M. I. Sezan and A. M. Tekalp, Efficient Multiframe Wiener Restoration of Blurred and Noisy Image Sequences, *IEEE Trans. Image Processing*, Vol. 1, No. 4, Oct. 1992, pp. 453-476.
- [18] R. W. Schafer, R. M. Mersereau and M. A. Richards, Constrained Iterative Restoration Algorithm, *Proc. of IEEE*, vol. 69, April 1981, pp. 432-450.
- [19] A. Tikhonov and V. Arsenin, *Solution of Ill-Posed Problems*, John Wiley and Sons, 1977.

- [20] M. E. Zervakis, Optimal restoration of multichannel images based on constrained mean square estimation, *Journal of Visual Communication and Image Representation*, Vol. 3, No. 4, Dec. 1992, pp. 392-411.
- [21] W. Zhu, N. P. Galatsanos and A. K. Katsaggelos, Regularized Multichannel Restoration using Cross-Validation *Graphics Models and Image Processing*, Vol. 57, No. 1, Jan. 1995, pp. 38-54.

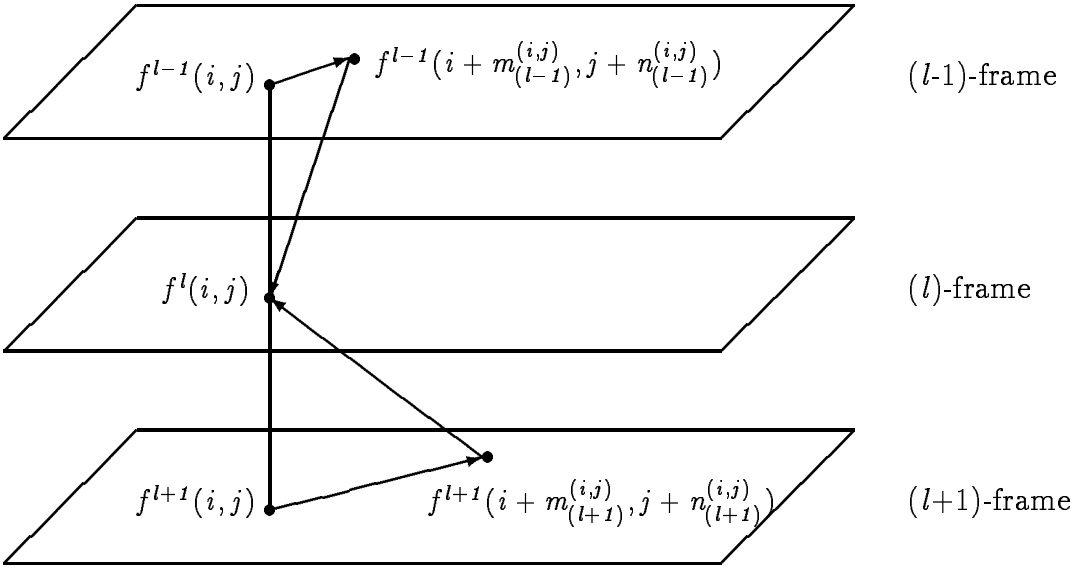


Figure 1: Between-Frame Pixel Correspondence in Image Sequences.

Figure 2 : ISNR plots ; Experiment I, case (i) : $BSNR = 10$ dB, 11×11 blur, $\alpha = 0.1$ and $\lambda = 0.1$.

Figure 3 : DFD plots ; Experiment I, case (i) : $BSNR = 10$ dB, 11×11 blur, $\alpha = 0.1$ and $\lambda = 0.1$.

(a)

(b)

(c)

(d)

Figure 4 : (a) Experiment *I* case (*i*), *DVF* plots between *twy047* and *twy048* frames, (a) using Model 1, (b) using Model 2, (c) using Model 3, and (d) using Model 4.

Figure 5 : ISNR plots ; Experiment I, case (ii) : $BSNR = 30$ dB, 11×11 blur, $\alpha = 2.0$ and $\lambda = 0.001$.

Figure 6 : DFD plots ; Experiment I, case (ii) : $BSNR = 30$ dB, 11×11 blur, $\alpha = 2.0$ and $\lambda = 0.001$.

(a)

(b)

(c)

(d)

Figure 7 : (a) Experiment I case (ii), *DVF* plots between *twy047* and *twy048* frames, (a) using Model 1, (b) using Model 2, (c) using Model 3, and (d) using Model 4.



(a)



(b)



(c)

Figure 8 : (a) Original Image(twy048), (b) Experiment I case (i): Degraded image, with 11×11 blur and 10 dB of *BSNR* additive noise. (c) Experiment I case (ii): Degraded image, with 11×11 blur and 30 dB of *BSNR* additive noise.



(a)



(b)



(c)



(d)

Figure 9 : (a) Experiment I case (i), restored images, (a) using Model 0, (b) using Model 1, (c) using Model 3, and (d) using Model 4.



(a)



(b)



(c)



(d)

Figure 10 : (a) Experiment I case (ii), restored images, (a) using Model 0, (b) using Model 1, (c) using Model 3, and (d) using Model 4.

Figure 11 : ISNR plots ; Experiment II : BSNR = 30 dB, variable zooming/panning with 11×1 motion blur, $\alpha = 2.0$ and $\lambda = 0.001$.

Figure 12 : *DFD* plots ; Experiment *II* : *BSNR* = 30 *dB*, variable zooming/panning with 11×1 motion blur, $\alpha = 2.0$ and $\lambda = 0.001$.



(a)



(b)

Figure 13 : (a) Original Image(twy046), (b) Experiment II : Degraded image, 11×1 motion blur, and 30 dB of *BSNR*, $\alpha = 2.0$ and $\lambda = 0.001$.



(a)



(b)



(c)



(d)

Figure 14 : Experiment II : restored images, (a) using Model 0, (b) using Model 1, (c) using Model 3, and (d) using Model 4.